

Mechanisms of magnetoelectricity in manganese doped incipient ferroelectrics

R.O. KUZIAN¹, V.V. LAGUTA^{1,2}, A.-M. DARÉ³, I.V. KONDAKOVA¹, M. MARYSKO², L. RAYMOND³, E.P. GARMASH¹, V.N. PAVLIKOV¹, A. TKACH⁴, P. M. VILARINHO⁴ and R. HAYN³

¹ *Institute for Problems of Materials Science NASU - Krzhizhanovskogo 3, 03180 Kiev, Ukraine*

² *Institute of Physics, AS CR - Cukrovarnicka 10, 16253 Prague, Czech Republic*

³ *Aix-Marseille Université, IM2NP CNRS - FST St-Jérôme, Avenue Escadrille Normandie Niemen, F-13397, Marseille Cedex, France*

⁴ *Department of Ceramics and Glass Engineering, CICECO, University of Aveiro - 3810-193 Aveiro, Portugal*

PACS 75.85.+t – Magnetoelectric effects, multiferroics

PACS 75.30.Hx – Magnetic impurity interactions

PACS 76. – Magnetic resonance

Abstract. - We report magnetization measurements and magnetic resonance data for SrTiO₃ doped by manganese. We show that the recently reported coexistent spin and dipole glass (multiglass) behaviours are strongly affected by the distribution of Mn ions between the Sr and Ti sites. Motivated by this finding we calculate the magnetic interactions between Mn impurities of different kinds. Both LSDA+*U* and many-body perturbation theory evidence that magnetic and magnetoelectric interactions are mediated by Mn_B⁴⁺ ions substituting for Ti. We propose two microscopic magnetoelectric coupling mechanisms, which can be involved in all magnetoelectric systems based on incipient ferroelectrics. In the first one, the electric field modifies the spin susceptibility via spin-strain coupling of Mn_B⁴⁺. The second mechanism concerns Mn pairs coupled by the position-dependent exchange interaction.

Introduction. – SrTiO₃ (STO) and KTaO₃ (KTO) doped by manganese have attracted considerable attention exhibiting simultaneous spin and dipole glass behaviours with large non-linear magnetoelectric coupling [1–3]. Such "multiglass" systems extend non-trivially the frame of conventional multiferroicity and give new perspective for studies of the phenomenon and potential application in microelectronic devices.

Both STO and KTO are special representatives of the perovskite family of ABO₃ materials. They are incipient ferroelectrics (IF), i.e. they remain paraelectric down to zero temperature, but exhibit very large dielectric permittivity (~ 20000 and 5000 respectively) at low temperature due to the softening of a transverse optical mode that corresponds to B sub-lattice oscillations with respect to the almost static rest of the lattice.

The Mn impurities in STO may substitute both for Sr and Ti; they will be denoted as Mn_A and Mn_B respectively. Isolated impurities are paramagnetic, Mn_B being an isotropic centre with formal valency Mn⁴⁺, and a spin $S = 3/2$ [4], while Mn_A which has valency 2+ and

$S = 5/2$, is isotropic at $T > 100$ K, and axial at low temperature [5]. According to the interpretation of ESR measurements [4,5], which were recently confirmed by density functional theory (DFT) calculations [6,7] and EXAFS experiments [8], the Mn_B impurity resides in the octahedrally coordinated cubic position B of the perovskite lattice, and Mn_A is displaced from A position thus forming electric dipoles in addition to magnetic ones.

Ceramic samples of STO doped by 2% of manganese exhibit spin- and polar- glass properties at temperature below $T_g \approx 38$ K. Moreover, a substantial non-linear magnetoelectric coupling was measured [1–3]. A similar behaviour for KTO:Mn system was also found [3]. The interaction of electric dipoles formed by off-central Mn_A impurities has the same nature as the interaction of other dipole impurities in IF, its mechanism is rather well understood [9]. In this paper we concentrate on magnetic and magnetoelectric interactions in STO:Mn. We show that the presence of off-central Mn_A²⁺ ions substituting for Sr is necessary but not sufficient to induce the multiglass behaviour, and that the magnetic interactions are medi-

ated by Mn_B^{4+} ions substituting for Ti.

Some aspects of the considered problem are interesting from the fundamental point of view. The interaction between ions with different d -shell filling and different spins connected by several bridging ligands requires a generalization of superexchange theory. The dependence of spin-Hamiltonian parameters on the external electric field is a non-trivial application of the ligand field theory for ions in a highly polarizable medium.

Experiment. – For our experimental studies we have used two groups of STO:Mn ceramic samples prepared in different labs. We will call them I and II. Type-I ceramics with the formal chemical composition $\text{Sr}_{0.98}\text{Mn}_{0.02}\text{TiO}_3$ were prepared by mixed oxide technology described elsewhere [10]. In particular, reagent grade SrCO_3 , TiO_2 and MnO_2 were mixed in appropriate amounts, ball milled, dried and calcined at 1100°C for 2 h. The calcined powders were again milled, pressed isostatically and sintered at 1500°C for 5 h. For the type-II ceramics (formal chemical composition $\text{Sr}_{0.96}\text{Mn}_{0.04}\text{TiO}_3$), instead of MnO_2 , powder of MnCO_3 was used. The calcination was performed at 1150°C for 4 h and the sintering at 1360°C for 2 h. Both types of samples possess Mn_A^{2+} off-central impurities and have similar dielectric properties, but as shown below their magnetic responses are strikingly different.

The magnetic measurements were performed using a SQUID magnetometre (MPMS-6S Quantum Design) in the temperature range 4.5 - 100 K. The zero-field-cooled (ZFC) and field-cooled (FC) susceptibilities were measured in an applied field of 100 Oe. The main experimental result of this paper is illustrated in Fig.1. While magnetic properties of type-I ceramics are similar to that reported in Refs. [1, 2], namely, they exhibit spin-glass behaviour at $T < 45$ K (Fig. 1a), the type-II ceramics remain paramagnetic down to liquid helium temperature (Fig. 1b). In addition, for the ceramics I the magnetization exhibits a hysteretic behaviour with a finite remanence and coercivity (Fig. 1c). On the contrary, the magnetic loops measured on ceramics II (Fig. 1d) show no hysteresis and remanence. In this case, the magnetization is almost entirely determined by the paramagnetic contribution.

In order to study the distribution of Mn ions in the lattice and their individual magnetic properties -they are the only source of magnetism in our system- we have performed ESR measurements at 9.2 GHz in the standard 3 cm wavelength range at temperatures from 4.2 up to 300 K. An Oxford instrument ESR 900 cryosystem was used. In both types of ceramics we have found the spectra of Mn_A^{2+} and Mn_B^{4+} ions, which were described in detail in our previous paper and other early publications (see, e.g. Refs. [4,5]). The main difference between the two types of ceramics revealed by ESR is the ratio of $\text{Mn}^{2+}/\text{Mn}^{4+}$ ion concentration, which is 70/30 and 90/10 for types I and II respectively, as shown in Fig. 1.e-h. The absolute concentration of Mn_A^{2+} in both ceramics is about $1 \div 1.3\%$ as the ceramics contain also some amount of MnTiO_3 inclu-

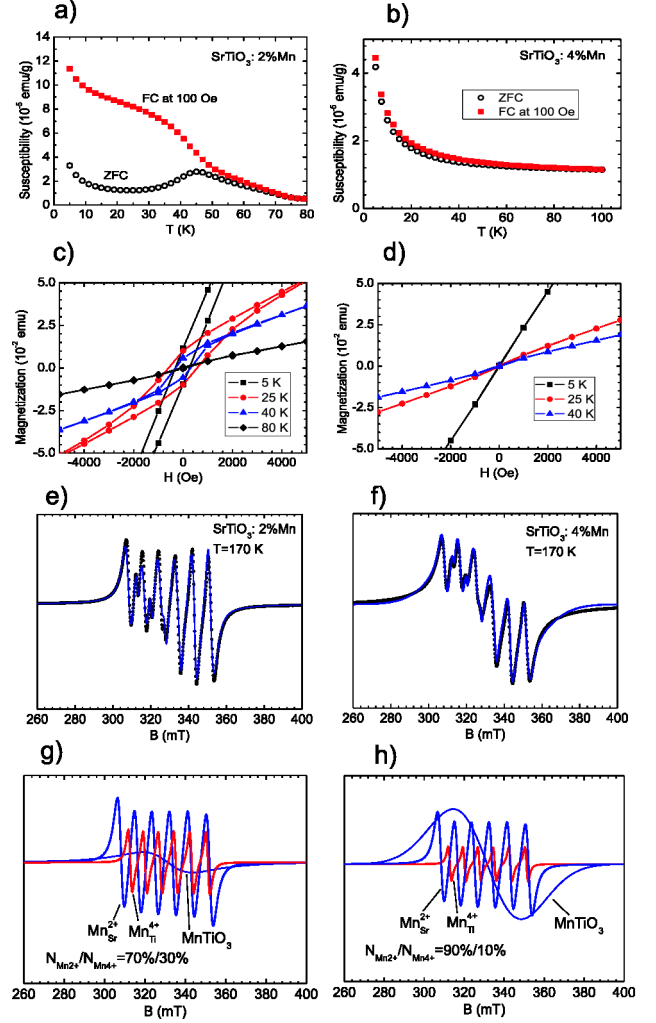


Figure 1: (Coloronline) Comparison of magnetic properties for ceramics I (left) and II (right). a),b) ZFC and FC susceptibilities as a function of temperature. Magnetization as a function of applied field, measured c) in type-I ceramics at 80, 40, 25, and 5 K, and d) in type-II ceramics at 40, 25, and 5 K. e),f) Experimental (dots) EPR spectra, and the corresponding simulations (solid lines). g),h) EPR spectra decomposition which shows the percentage of various Mn paramagnetic centres.

sions reflected in ESR spectra by a broad line (see, Fig. 1 g,h) and observed previously in electron diffraction spectra (Ref. [10]). Although in the type-II ceramics about 70% of Mn ions contribute to this MnTiO_3 fraction, it does not markedly influence the magnetic properties of the studied samples (Figs. 1b,1d) due to relatively small magnetic anomaly of MnTiO_3 at the antiferromagnetic phase transition at 63 K (Ref. [11]).

DFT calculations. – We have theoretically studied the interactions between Mn ions using LSDA+ U and many-body perturbation theory. We have considered the Mn impurities when they occupy nearest neighbour positions, and looked at the various pairs $\text{Mn}_A\text{-Mn}_A$, $\text{Mn}_A\text{-Mn}_B$, and $\text{Mn}_B\text{-Mn}_B$. The Mn_A ions were shifted in var-

Table 1: Hamiltonian (1) parameters calculated with LSDA+ U for various configurations of Mn_A^{2+} - Mn_A^{2+} pair in a $2 \times 2 \times 3$ 60 atom supercell (symmetry group P4mm, #99); $U = 4$ eV

$d_1, \text{\AA}$	$d_2, \text{\AA}$	E_n, meV	J_{AA}, meV
0	0	0	-0.008
0.82	0.82	-695.5	0.23
0.35	-0.35	-26.6	0.46
-0.47	0.47	-27.2	0.04

ious directions from the symmetric A position.

Density functional theory calculations were performed using the full-potential local-orbital (FPLO) code [12]. The total energies for different configurations were obtained, and the results were mapped onto an Mn-Mn pair effective Hamiltonian of the form

$$\hat{H} = E_n(\mathbf{d}_1, \mathbf{d}_2) + J_{12}(\mathbf{d}_1, \mathbf{d}_2) \hat{\mathbf{S}}_1 \hat{\mathbf{S}}_2, \quad (1)$$

where \mathbf{d}_i is the shift from cubic position. E_n is a non-magnetic spin-independent interaction, treating the ion motion classically, it is a c -number in our approach. The spin part of the interaction is of Heisenberg-type.

We present the results for Mn_A^{2+} - Mn_A^{2+} pairs in Table 1. Various Mn_A^{2+} displacements along the symmetry axis Z were considered: $d_1 = d_2$ (the ions shift conserving the distance between them), $d_1 = -d_2 > 0$ (ions shift towards each other), $d_1 = -d_2 < 0$ (away from each other). In each case the results correspond to the total energy minima with respect to displacement. The non shifted distance between two A sites is 3.9 \AA [6].

The third column shows that the configuration with parallel shift of Mn ions ($d_1 = d_2 = 0.82 \text{ \AA}$) is separated from the others by such a large energy, that these will not be observed within the physically relevant temperature range. A similar situation was described in Ref. [15] for Li-Li pairs in KTaO_3 . The last column of Table 1 represents one of the main theoretical findings of this work, namely, it shows that the magnetic interaction of nearest neighbour Mn_A^{2+} ions, for the most probable parallel configuration, satisfies $|J_{AA}/k_B| < 3$ K. In fact this value is on the verge of precision of DFT calculations. Despite the large spin value of Mn_A^{2+} ions, this interaction cannot be responsible for magnetic susceptibility anomalies at $T \sim 40$ K that we observe for type I ceramics (Fig.1), and that were reported in previous studies of STO:Mn [1, 2].

Table 2 shows the results for a Mn_A^{2+} - Mn_B^{4+} pair. Here the Mn_A^{2+} ion shift was taken to be the same as the one found for the isolated ion [6]; for $d_A > (<)0$ the ions get farther (closer). Finally, for the pair Mn_B^{4+} - Mn_B^{4+} we have found $J_{BB} = 9.3$ meV, i.e. $J_{BB}/k_B = 107.9$ K. So, we may conclude that the presence of Mn_B^{4+} ions may be responsible for the observed anomalies in magnetic susceptibilities.

Theory of superexchange. – To reach a better understanding of the exchange mechanism we have per-

Table 2: Hamiltonian parameters for Mn_A^{2+} - Mn_B^{4+} pair, calculated for a $2 \times 2 \times 2$ 40 atom supercell (P1, #1); $U = 4$ eV

$d_A, \text{\AA}$	E_n, meV	J_{AB}, meV	$J_{AB}/k_B, \text{K}$
0	0	0.5	5.8
-0.64	-144.6	1.65	19.1
0.64	-123.02	0.51	5.9

formed analytic calculations of the superexchange interaction between Mn ions within fourth-order many-body perturbation theory. Using resolvent method [16] we obtained a general formula for the magnetic coupling between two spins S_1 and S_2 in terms of hopping integrals $t_{im\beta n}$ between cations (im) (i specifies the cation, m the orbital index) and neighbouring ligands (βn) (β specifies the ligand, n the orbital). Taking the hole point of view (no fermion on the ligand p orbitals in the ground state) we have established Eq.(2), where the sum over the cation orbitals m and m' is restricted to ground-state occupied ones (abbreviation "occ"). $\Delta_{i\beta n}$ is the energy of the excited state (measured with respect to the ground state), where one fermion has moved from (im) to (βn), while Δ_{ij} is the difference of energy between an excited state with $N_i - 1$ and $N_j + 1$ fermions on cation i and j respectively, and the ground state (GS) with N_i and N_j fermions per cation respectively. If the cations are of the same type, one has $\Delta_{ij} = \Delta_{ji}$ and $\Delta_{i\beta n}$ does not depend on i . The three added terms inside the bracket in Eq.(2) correspond to different paths: the first two involve intermediate excited states with $(N_i - 1, N_j + 1)$ fermions on the cations, while the third term corresponds to an excited state with two fermions on the ligands with repulsion U_p when the holes meet on the same ligand.

The parameters $t_{im\beta n}$, $\Delta_{i\beta n}$ and Δ_{ij} were extracted from the analysis of photoemission experiments reported in Refs. [17, 18]. We denote for the BB-pair: $\Delta_{12} = U_{eff}^B$, $\Delta_{i\beta n} = \Delta_{eff}^B$; for the AA-pair $\Delta_{12} = U_{eff}^A$, $\Delta_{i\beta n} = \Delta_{eff}^A$; while for the BA-pair $\Delta_{12} = \Delta_{eff}^B - \Delta_{eff}^A + U_{eff}^A$, $\Delta_{21} = \Delta_{eff}^A - \Delta_{eff}^B + U_{eff}^B$, $\Delta_{1\beta n} = \Delta_{eff}^B$, and $\Delta_{2\beta n} = \Delta_{eff}^A$, where $\Delta_{eff}^i = \Delta_i + J_{Hi} [7/9(N_i - 1) - p_i]$ and $U_{eff}^i = U_i + J_{Hi} [N_i + 11/9 - 2p_i]$, with $J_{Hi} = 5/2B_i + C_i$, N_i is the number of holes in the ground state of Mn_i ion and p_i is the number of doubly-occupied orbitals. We use the following experimental values (in eV) for Mn_B : $B_i = 0.132$, $C_i = 0.610$, $\Delta_i = 2 \pm 0.5$ and $U_i = 7.5 \pm 0.5$ (Table I of Ref. [17].), while for Mn_A , $B_i = 0.119$, $C_i = 0.412$, $\Delta_i = 7$ and $U_i = 5.5$ (Table I, II of Ref. [18]). This gives $\Delta_{eff}^A = 9.2$ eV, $\Delta_{eff}^B = 4.5 \pm 0.5$ eV, $U_{eff}^A = 9.9$ eV and $U_{eff}^B = 11.6 \pm 0.5$ eV. The hopping parameters are expressed in terms of Slater-Koster parameters [19] $V_{pd\pi, \sigma}^{A(B)}$ for $\text{Mn}_{A(B)}$, they essentially depend on the cation-ligand distance, we take $V_{pd\sigma}^i/V_{pd\pi}^i = -2.16$ [19]. Following Ref. [18], we have assumed that the hopping which links states

$$\begin{aligned}
J = & \frac{1}{2S_1S_2} \sum_{\beta\beta'nn'} \sum_{mm'}^{occ} t_{1m\beta n} t_{2m'\beta n} t_{1m\beta'n'} t_{2m'\beta'n'} \left\{ \frac{1}{\Delta_{1\beta n} \Delta_{1\beta'n'} \Delta_{12}} + \frac{1}{\Delta_{2\beta n} \Delta_{2\beta'n'} \Delta_{21}} \right. \\
& \left. + \frac{1}{\Delta_{1\beta n} + \Delta_{2\beta'n'} + U_p \delta_{\beta\beta'}} \left(\frac{1}{\Delta_{1\beta n}} + \frac{1}{\Delta_{2\beta'n'}} \right) \left(\frac{1}{\Delta_{2\beta n}} + \frac{1}{\Delta_{1\beta'n'}} \right) \right\}, \quad (2)
\end{aligned}$$

Table 3: Superexchange values $j_{BA} = J_{BA}/J_{BB}$, and $j_{AA} = J_{AA}/J_{BB}$ with $J_{BB} = (9.5 \pm 1.5)(V_{pd\pi}^B)^4$ for different A-shift.

d_A	j_{BA}	$j_{BA},$ LSDA+U	j_{AA}	$j_{AA},$ LSDA+U
0	0.39	0.054	0.008	-0.001
0.82			0.008	0.025
-0.64	0.52	0.177		
0.64	0.29	0.055		

with $N + 1$ and N holes on some cation, is reduced by a factor R compared to hopping linking states with $N - 1$ and N holes. The results (and their comparison with LSDA+U) are presented in Table 3 for the parameters $R = 1.2$ and $U_p = 4$ eV, and the shifts are the same as those found in LSDA calculations.

As can be seen, the agreement is qualitative between perturbative calculations and DFT results. In addition, the super-exchange theory enables to discuss various tendencies and contributions. The different exchange coupling J_{BB} , J_{AB} and J_{AA} are proportional to $(V_{pd\pi}^B)^4$, $(V_{pd\pi}^A)^2(V_{pd\pi}^B)^2$ and $(V_{pd\pi}^A)^4$ respectively. A crude estimate based on the different distances, leads to $J_{AB}/J_{BB} \sim 0.1$ and $J_{AA}/J_{BB} \sim 0.01$. One can also expect a predominant value for J_{BB} due to geometry: it corresponds to a 180° Mn_B-O-Mn_B link, while the other two are 90° ones. The difference between exchange couplings are also due to different number of exchange paths and to difference in charge transfer values $\Delta_{eff}^A > \Delta_{eff}^B$. The number of paths for J_{AA} is larger than for the other two, since four ligands and many orbitals come in, against three ligands for J_{AB} and only one for J_{BB} . Two or more ligands raise the opportunity to have ferromagnetic contributions, which explains reduction of J_{AA} compared to the other two, further than what was expected just by distance effect.

Mechanisms of magnetoelectric coupling. –

We propose two possible mechanisms involving Mn_B⁴⁺ ions, which may be relevant for IF doped by manganese. In the following we consider the solid solution Sr_{1-x}Mn_xTi_{1-y}Mn_yO₃. The magnetoelectricity implies the dependence of the magnetic susceptibility on an electric field. Up to second order, the magnetic susceptibility

may be written

$$\chi_{ij} = - \left. \frac{\partial^2 F}{\partial H_i \partial H_j} \right|_{H=0} = \chi_{0,ij} + \chi_{1,ijk} E_k + \chi_{2,ijkl} E_k E_l. \quad (3)$$

where the free energy density F , the magnetic and electric field components, H_i and E_i are measured in CGS units. To translate this equation in terms of Ref. [2] notations with SI units, one should use the relations

$$\begin{aligned}
\beta_{ijk} &= (4\pi)^{\frac{3}{2}} \mu_0 \sqrt{\varepsilon_0} \chi_{1,ijk} \approx 1.67 \cdot 10^{-10} \chi_{1,ijk} \text{ s/A} \quad (4) \\
\delta_{ijkl} &= 8\pi^2 \mu_0 \varepsilon_0 \chi_{2,ijkl} \approx 8.78 \cdot 10^{-16} \chi_{2,ijkl} \text{ sm/VA} \quad (5)
\end{aligned}$$

The first mechanism is a one-spin effect: The polarization P of the lattice, is accompanied by a lattice strain, which is proportional to the square of polarization [20]. The Mn_B⁴⁺ ion has a $3d^3$ configuration and a 4F GS, which is split by the ligand field in contrast to the $3d^5$ configuration and 6S GS for Mn_A²⁺. In a cubic field the Mn_B⁴⁺ ion has a fourfold degenerate 4A_2 GS. When the local symmetry becomes axial, an additional splitting arises. Its magnitude depends on the polarization via the strain. This affects the magnetic susceptibility. In a paraelectric phase, the changes are proportional to the square of the external electric field, but in the presence of a net polarization P_T in a polar phase, a linear dependence appears. Let us note that this mechanism will be effective in any ferroelectric perovskite doped by paramagnetic ions located at B sites and having the $3d^3$ configuration.

The contribution of this mechanism to the magnetoelectric susceptibility is given below by Eqs.(9) and (10). Substitution of numerical values relevant to the experimental conditions of Ref. [2] gives

$$\chi_{1,zzz} \approx -2.2 \cdot 10^{-9}, \quad \beta \approx -3.6 \cdot 10^{-19} \text{ s/A}, \quad (6)$$

$$\chi_{2,zzzz} \approx -1.2 \cdot 10^{-10}, \quad \delta \approx -0.1 \cdot 10^{-24} \text{ sm/VA}. \quad (7)$$

In these estimates, we have used $x + y = 0.02$, and $x/y \approx 70/30$, as found in our ESR experiment. The reported experimental values are [2] $\beta \approx -3 \cdot 10^{-19}$ s/A and $\delta \approx -9 \cdot 10^{-24}$ sm/VA. We see that the paramagnetoelectric susceptibility β is in fairly good agreement, but the biquadratic coefficient is underestimated by this mechanism which cannot be the only argument put forward.

The second mechanism concerns Mn_A-Mn_B pairs. As can be seen from Tables 2 and 3, the Mn_A²⁺ has non-equivalent equilibrium positions in the cell where Mn_B⁴⁺ is present. The superexchange interaction between Mn_B⁴⁺ and Mn_A²⁺ strongly depends on the displacement d_A .

Compared to the closer situation, the case with ions far from each other corresponds to a higher energy ΔE . As shown in detail in the following section, the lattice polarization increases the number $N_2(P_r, E)$ of Mn_A^{2+} ions lying farther from Mn_B^{4+} ions. This leads to a positive $\chi_{1,zzz}$. In the next section we show that this mechanism seems to be unimportant for the system studied in Ref. [2], but it may be very effective for a system where the interaction energy between electric Mn_A^{2+} -dipole and P_r is comparable with ΔE .

Calculation of non-linear magneto-electric susceptibility. – Here we quantitatively consider the ideas outlined in the previous section. This section is a little technical and can be safely skipped by someone not interested in the details of computation.

The first mechanism. In order to estimate its contribution, we follow the ideas of Ref. [21]. The Mn_B^{4+} ion is much more sensitive to the local strain than Mn_A^{2+} . In an octahedral coordination it has a 4A_2 orbital singlet ground state, and the effective spin 3/2 Hamiltonian has the form

$$\hat{H}_B = \mu_B g_{zz} H_z \hat{S}_z + \mu_B g_{\perp} (H_x \hat{S}_x + H_y \hat{S}_y) + D \left[\hat{S}_z^2 - \frac{1}{3} S(S+1) \right] - \mu_B^2 \sum_{\mu\nu} \Lambda_{\mu\nu} H_{\mu} H_{\nu}, \quad (8)$$

where $g_{\mu\nu} = g_s - 2\lambda k \Lambda_{\mu\nu}$, $D = -\lambda^2 (\Lambda_{zz} - \Lambda_{xx})$, $\Lambda_{\mu\nu} = \sum_{n \neq 0} \frac{\langle \psi_0 | \hat{L}^{\mu} | n \rangle \langle n | \hat{L}^{\nu} | \psi_0 \rangle}{E_n - E_0}$, $g_s = 2.0023$ is the spin gyromagnetic ratio, λ the spin-orbit coupling constant, $|\psi_0\rangle (|n\rangle)$ is the ground(excited) state, E_0 and E_n are the corresponding energies, \hat{L}^{μ} is the μ -th component of the orbital moment operator, k is the orbital reduction factor. Using the ligand field theory [22,23], which perturbatively takes into account $p-d$ hybridization between paramagnetic ion and surrounding ligands, we may obtain [24]

$$\begin{aligned} \Lambda_{zz} &= -\Delta g_{cub} (1 - \kappa e_{33}) / 2\lambda, \\ \Lambda_{xx} &= -\Delta g_{cub} (1 - 5\kappa e_{33}/2) / 2\lambda, \end{aligned}$$

where $\Delta g_{cub} = g_{cub} - g_s$ refers to the g -value for undistorted cubic lattice, $\kappa \sim -3.5, -4$ is the exponent of $p-d$ hopping dependence on distance [19]. The dependence on electric field of the previous equations is only in the strain e_{33} . For multiglass samples we may assume that both, the net polarization P_r and the electric field are directed along the axis Z , while $\mathbf{P} = \mathbf{P}_r + (\varepsilon - 1) \mathbf{E} / 4\pi$. With an external magnetic field also applied along the Z -axis, we compute the partition function Z_B and the free energy density $F_B = -(y/v_c)\theta \ln Z_B$, with y/v_c the density of Mn_B^{4+} ions, v_c the host lattice unit cell volume and $\theta \equiv k_B T$. From this free energy, we finally derive the linear contribution to the magnetic susceptibility (Eq.(3)):

$$\chi_{1,zzz} \approx -\frac{y}{v_c} \mu_B^2 \Lambda'_{zz} \left\{ \frac{g_{zz}\lambda}{\theta} \left[5k + \frac{3g_{zz}\lambda}{2\theta} \right] - 2 \right\}, \quad (9)$$

where we have taken into account that $D/\theta \ll 1$ for $T = 10$ K. The (double)-prime indicates the (second)-

derivative with respect to E . Similarly, for the second order contribution, we have

$$\begin{aligned} \chi_{2,zzzz} &\approx \frac{y\mu_B^2}{v_c} \left\{ k (\lambda \Lambda'_{zz})^2 [10k + 12g_{zz}\lambda/\theta] / \theta \right. \\ &\quad \left. - \Lambda''_{zz} \left[\frac{g_{zz}\lambda}{\theta} \left(5k + \frac{3g_{zz}\lambda}{2\theta} \right) - 2 \right] \right\}. \quad (10) \end{aligned}$$

When we substitute $\kappa = -3.5$, $g_{cub} = 1.992$ [5], $\lambda \approx 135$ cm^{-1} , [25], $k \approx 1$, SrTiO₃ lattice parameter $a = 3.9$ \AA , ($v_c = a^3$), and $c/a \approx 1.002$ [6], $\varepsilon(T = 10 \text{ K}) \approx 1500$, and a net polarization $P_r \approx 0.7$, $\mu\text{C}/\text{m}^2 = 2100$ esu/cm^2 [10], we obtain the values presented in Eqs. (6) and (7).

The second mechanism. It involves a pair of Mn_A - Mn_B ions. There are six available positions for Mn_A , three

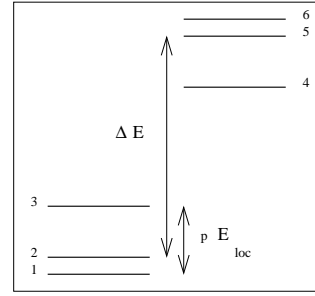


Figure 2: Changes of Mn_A - Mn_B pair energies in polarized medium. Here $E_{loc} = E + \frac{4\pi}{3}\gamma P$ is positive, however it can be negative, depending on the relative direction of polarization with respect to the pair Mn_A - Mn_B . The Lorentz factor γ accounts for the deviation of the local field from the simple cubic case, $p \approx Z_A d_A$ is the dipole moment of Mn_A^{2+} , $Z_A \approx 2$ is its dynamic charge.

of them are closer to Mn_B^{4+} and lower in energy: the number of Mn_A^{2+} in deep (shallow) wells is $N_{1(2)}$. Writing $N_1 = n_1 + n_2 + n_3$, and $N_2 = n_4 + n_5 + n_6$, one has in absence of polarization $N_2/N_1 = \exp(-\Delta E/\theta)$. However with polarization, there is some lift of degeneracy, as can be seen on Fig. 2, this leads to a redistribution of level occupancies, and $N_{1(2)}$ acquires a dependence on the net polarization P_r and on the external electric field E . With $N_1 + N_2 = xyz$, ($z = 8$ is the coordination number), the susceptibility reads

$$\chi = \chi_0 + \chi_1 xyz + (\chi_2 - \chi_1) N_2(P_r, E), \quad (11)$$

where χ_0 comes from contribution of everything but Mn_A - Mn_B pairs, while $\chi_J (J = 1, 2)$ is the susceptibility of a pair $S_A = 5/2 - S_B = 3/2$ coupled by the exchange interaction $J_{AB}(d_A)$, which depends on the Mn_A position [26]. The dependence of χ on the electric field comes from $N_2(P_r, E)$. Defining $n(t) \equiv (2 + e^{-t})/(2 + e^t)$, one has

$$N_2(P_r, E) = \frac{xyz}{2} \left[\frac{1}{n(t)e^{\Delta E/\theta} + 1} + \frac{1}{n(-t)e^{\Delta E/\theta} + 1} \right] \quad (12)$$

with $t = pE_{loc}/\theta$, $pE_{loc} \approx cE + \Delta_r$, $c = p\varepsilon\gamma/3$ and $\Delta_r = 4\pi\gamma p P_r/3$, ($\varepsilon \gg 1$ was used). See the caption of Fig. 2 for

definitions. Finally, making a limited development up to second order in electric field E , we obtain

$$\chi_{1,zzz} = (\chi_2 - \chi_1) N_2'(P_r, 0), \quad (13)$$

$$\chi_{2,zzzz} = (\chi_2 - \chi_1) N_2''(P_r, 0). \quad (14)$$

Substituting the values from Table 2: $\Delta E \approx -123 + 144.6 = 21.6$ meV, $J_1 \approx 1.7$ meV, $J_2 \approx 0.5$ meV, and $\gamma \approx -0.2$ [9], this gives $\Delta_r \approx -14$ meV, and a very tiny contribution of this second mechanism to the susceptibilities $\chi_1 \approx 7.1 \cdot 10^{-15}$, $\chi_2 \approx 1.6 \cdot 10^{-15}$. However, since N_2' is strongly dependent on $\Delta E - \Delta_r$, the second mechanism could be of the same order than the first one or even exceed it for $\Delta E \approx \Delta_r$ (then $\chi_1 \approx 4.6 \cdot 10^{-7}$, $\chi_2 \approx 1.7 \cdot 10^{-7}$): this equality can be realized for other concentrations of manganese in SrTiO₃ host, or for other systems (e.g. K_{1-x}Mn_xTa_{1-y}Mn_yO₃ [3]).

Summary. – We have compared the magnetic properties of two types of ceramic samples of manganese doped SrTiO₃. Based on the data of ESR measurements we conclude that the spin-glass behaviour is observed only in samples containing an appreciable percentage of Mn_B⁴⁺ ions substituting for Ti, in addition to Mn_A²⁺ substituting for Sr. Using LSDA+ U supercell calculation we have shown that the exchange interaction between Mn_A²⁺ impurities is an order of magnitude smaller than those for Mn_B⁴⁺-Mn_A²⁺ and Mn_B⁴⁺-Mn_B⁴⁺ pairs. The analytic many-body calculations have shown that the reason for this difference is the interference of various exchange paths for the Mn_A²⁺-Mn_A²⁺ pairs combined with different geometry, Mn-O distances, and stability of the Mn_A²⁺ ground state configuration in comparison to other pairs. We conclude that the presence of Mn_B⁴⁺ ions is essential for the formation of a collective magnetic state at low temperature. We propose two microscopic mechanisms of magnetoelectricity in SrTiO₃:Mn which involve Mn_B⁴⁺ ions.

* * *

The authors thank M.D. Glinchuk for fruitful discussions, the PICS program (Contracts CNRS No. 4767, NASU No. 267) and grant MSMT CR (Project No. 1M06002) for financial support and the IFW Dresden (Germany) which allowed us to use their computer facilities. The institutional research plan AVOZ10100521 is acknowledged.

References

- [1] KLEEMANN W., SHVARTSMAN V. V., BEDANTA S., BORISOV P., TKACH A. and VILARINHO P. M., *J. Phys.: Cond. Matt.*, **20** (2008) 434216.
- [2] SHVARTSMAN V. V., BEDANTA S., BORISOV P., KLEEMANN W., TKACH A. and VILARINHO P. M., *Phys. Rev. Lett.*, **101** (2008) 165704
- [3] KLEEMANN W., BEDANTA S., BORISOV P., SHVARTSMAN V. V., MIGA S., DEC J., TKACH A. and VILARINHO P. M., *Eur. Phys. J. B*, **71** (2009) 407
- [4] MULLER K.A., *Phys. Rev. Lett.*, **2** (1959) 341; MULLER K. A., and BURKARD H., *Phys. Rev. B*, **19** (1979) 3593
- [5] LAGUTA V. V., KONDAKOVA I. V., BYKOV I. P., GLINCHUK M. D., TKACH A., VILARINHO P. M., and JASTRABIK L., *Phys. Rev. B*, **76** (2007) 054104
- [6] KONDAKOVA I. V., KUZIAN R. O., RAYMOND L., HAYN R., and LAGUTA V. V., *Phys. Rev. B*, **79** (2009) 134117
- [7] O. E. KVYATKOVSKI, *Phys. Solid State*, **51** (2009) 982
- [8] LEVIN I., KRAYZMAN V., WOICIK J. C., TKACH A., and VILARINHO P. M., *Appl. Phys. Lett.*, **96** (2010) 052904
- [9] VUGMEISTER B. E. and GLINCHUK M. D., *Rev. Mod. Phys.*, **62** (1990) 993
- [10] TKACH A., VILARINHO P. M., and KHOLKIN A. L., *Appl. Phys. Lett.*, **86** (2005) 172902; TKACH A., VILARINHO P. M., and KHOLKIN A. L., *Acta Mater.*, **53** (2005) 5061
- [11] STICKLER J.J., KERN S., WOLD A., and HELLER G.S., *Phys. Rev.*, **164** (1967) 765
- [12] FPLO-7.00-28 (improved version of the original FPLO code by KOEPERNIK K. and ESCHRIG H., *Phys. Rev. B*, **59** (1999) 1743; <http://www.FPLO.de>). The exchange and correlation potential of Perdew and Wang [13] was employed as well as the FPLO implementation of LSDA+ U method in the atomic limit scheme [14].
- [13] PERDEW J. P. and WANG Y., *Phys. Rev. B*, **45** (1992) 13244
- [14] ESCHRIG H., KOEPERNIK K., and CHAPLYGIN I., *J. Solid State Chem.*, **176** (2003) 482
- [15] PROSANDEEV S.A., COCKAYNE E., and BURTON B.P., *Phys. Rev. B*, **68** (2003) 014120
- [16] AUERBACH A., *Interacting electrons and quantum magnetism* (Springer-Verlag) 1994
- [17] BOCQUET A. E., MIZOKAWA T., SAITOH T., NAMATAME H., and FUJIMORI A., *Phys. Rev. B*, **46** (1992) 3771
- [18] MIZOKAWA T., and FUJIMORI A., *Phys. Rev. B*, **48** (1993) 14150
- [19] HARRISON W.A., *Electronic structure and the Properties of Solids* (Freeman (San Francisco)) 1980
- [20] RIMAI L. and DEMARS G. A., *Phys. Rev.*, **127** (1962) 702
- [21] HOU S. L. and BLOEMBERGEN N., *Phys. Rev.*, **138** (1965) A1218
- [22] KUZMIN M.D., POPOV A.I., and ZVEZDIN A.K., *Phys.Stat. Sol. (b)*, **168** (1991) 201
- [23] KUZIAN R.O., DARÉ A.M., SATI P., and HAYN R., *Phys. Rev. B*, **74** (2006) 155201
- [24] GLINCHUK M.D., and KUZIAN R.O., *Physica B*, **389** (2007) 234
- [25] ABRAGAM A. and BLEANEY B., *Electron Paramagnetic Resonance of Transition Ions* (Clarendon, Oxford) 1970, p. 437
- [26] We have

$$\chi_J = \sum_{S=|S_A-S_B|}^{|S_A+S_B|} \frac{(2S+1) \exp(-E_S/\theta)}{\sum_{S'} (2S'+1) \exp(-E_{S'}/\theta)} \chi_S \quad (15)$$
 with $E_S = \frac{1}{2} J_{AB} [S(S+1) - S_A(S_A+1) - S_B(S_B+1)]$, the magnetic energy of the pair corresponding to the total spin S , $\chi_S = (\mu_B g_S)^2 S(S+1) / (3v_c \theta)$ is the corresponding magnetic susceptibility, and the gyromagnetic ratio is $g_S = \frac{1}{2} \left[g_A + g_B + (g_A - g_B) \frac{S_A(S_A+1) - S_B(S_B+1)}{S(S+1)} \right]$.